

Extreme ultraviolet plasmonics and Cherenkov radiation in silicon: supplementary material

PRASHANT SHEKHAR^{1,2,3}, SARANG PENDHARKER⁴, HARSHAD SAHASRABUDHE⁵, DOUGLAS VICK⁶, MAREK MALAC⁶, RAJIB RAHMAN³, AND ZUBIN JACOB^{1,2,3,*}

¹Department of Electrical and Computer Engineering, University of Alberta, Canada

²Birck Nanotechnology Center, Purdue University, USA

³School of Electrical and Computer Engineering, Purdue University, USA

⁴Department of Electronics and Electrical Communication Engineering, Indian Institute of Technology, Kharagpur, West Bengal, India

⁵Department of Physics and Astronomy, Purdue University, USA

⁶Nanotechnology Research Centre, Nat. Res. Council, Alberta, Canada

*Corresponding author: zjacob@purdue.edu

Published 7 December 2018

This document provides supplementary information to "Extreme ultraviolet plasmonics and Cherenkov radiation in silicon," <https://doi.org/10.1364/OPTICA.5.001590>.

1. METHODS

A. *k*-EELS Setup and Methodology

k-EELS measurements require a notably different setup of the TEM compared to momentum-integrated EELS or STEM-EELS techniques (figure 2(a)). An Hitachi HF-3300 TEM/STEM with a cold field emission gun (CFEG) and a Gatan Image Filter (GIF) TridiemTM and the MAESTRO central computer control system [1] were used to conduct the *k*-EELS measurements. The TEM is aligned and configured to have a parallel electron beam (with a 0.1 μm diameter probe) at the sample plane with a 300 keV incident energy. A parallel beam with a large probe diameter is required in order to map the *k*-space dispersion of the excitations, which is in direct contrast to the point like probe of STEM-EELS used for high spatial resolutions. Electrons with normal incidence pass through the sample and are scattered with a momentum transfer (Δk) and undergo an energy loss ($\Delta E = \hbar\omega$) corresponding directly to the momentum and energy of excitations in the sample with resolutions of $\approx 0.03 \mu\text{rad}/\text{channel}$ and $\approx 0.01 \text{ eV}/\text{channel}$, respectively down to $\approx 1.2 \text{ eV}$ until the ZLP onset. Inelastically scattered electrons at an angle θ over a range of $-30 \mu\text{rad}$ to $30 \mu\text{rad}$ in the k_x direction were selected by an EELS slit in the diffraction plane. Additionally, the electron energy loss over a range of 0-18 eV was resolved via the EEL spectrometer and the corresponding momentum-energy loss of the electrons were mapped to the calibrated CCD.

The *k*-EELS experiment was performed in diffraction mode with a 3 meter camera length and the sample was illuminated with a 0.1 μm diameter probe. GIF alignment procedures were conducted using a series of energy selecting slits ranging from 40

eV to 2 eV and tuned to have non-isochromaticity to 1st and 2nd order well below tolerance (0.07 eV and 0.32 eV, respectively). Although the total GIF alignment was performed (including tuning for image distortions, achromaticity, and magnification), no energy selecting slit was used during the *k*-EELS acquisition. The parallel illumination allows for the entire *k*-EELS energy-momentum map image to be recorded for each sample using a 1 second acquisition time integrated over 5 images in the GIF spectroscopy mode. As the silicon thin films have isotropic plasmonic properties in *k*-space the direction of critical points of the Brillouin zone were not considered however electrons were traveling perpendicular to the (100) silicon crystal plane.

B. Uncertainty in Measurement

It is evident from figure 2(b) in the main manuscript that there is an increased uncertainty in the *k*-EELS measurement at larger scattering angles. This is a result of the decreased signal to noise ratio (SNR) of the EELS measurement at large scattering angle (large *k*) due to the inherent *k*-space scaling of of EELS signal intensity (figure 3).

Furthermore, an increased uncertainty is observed in the surface contributions (the SP) as compared to the bulk contributions (the BP) in figure 2(b) as the scattering angle increases. This is due to the fact that the surface scattering intensity decreases with scattering angle exponentially faster than bulk contributions (k^{-3} versus k^{-2} , respectively) (figure 3). This leads to a relatively lower SNR for the surface contributions compared to bulk contributions leading to increased uncertainty for surface contributions at larger *k*.

Additionally, an overall increase in the measurement uncer-

tainty is observed for thinner films as compared to the thicker silicon films. This is a result of the inelastic mean free path of silicon (≈ 180 nm for 300 keV electrons) being much larger than the film thickness leading to a decreased inelastic scattering signal intensity for the thinner films.

C. DFT Calculations using the GW Approximation

The dielectric constant is calculated using the GW approximation in the Vienna Ab initio simulation package (VASP [2]), where G is the single particle Green's function, and W is the screened Coulomb interaction between electrons. Quasiparticle energies and wavefunctions corresponding to unoccupied orbitals (bands) are obtained using this method. The dielectric constant is then evaluated using the wavefunctions and their derivatives with respect to momentum. In this approximation, the self-energy (Σ) of the many-body electron system is truncated to the first order in G . A partially self-consistent method (GW_0 algorithm in VASP) is used, which is shown to closely match experiments, where G and Σ are updated until convergence and W is fixed.

Interestingly our calculations using the Bethe-Salpeter Equation (BSE), which describe electron-hole bound states, calculates the experimental permittivity of silicon well at lower energies but begins to deviate at energies into the UV regime and higher (figure S1). Conversely, the DFT with the GW approximation shows a much stronger match to the experimental data at high energies (figure 1 (b) of the main manuscript) which suggests that the electron-hole pairs are not strongly bound but move freely at higher energies.

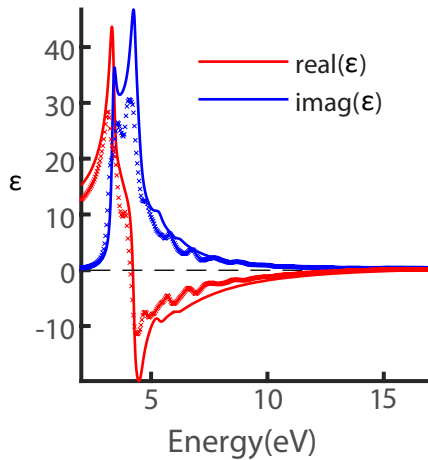


Fig. S1. Bethe-Salpeter Equation (BSE) calculations of the dielectric permittivity of silicon. Experimental silicon permittivity data (solid lines) [3] and our BSE calculations predicting the dielectric permittivity of silicon (x). BSE, which describes electron-hole bound pairs, agrees well at lower energies where electron and holes are tightly bound but begins to deviate at energies into the UV regime and higher. Conversely, the DFT with the GW approximations (figure 1 (b) of the main manuscript) agrees strongly with the experimental data in this region which suggests that electrons are not strongly bound in this region but can move freely. This increase in the free charge density is a result of less tightly bound electron-hole pairs and is what leads to silicon's metallic character in the EUV.

2. CHERENKOV RADIATION IN SILICON THIN FILMS

Silicon has been observed to support Cherenkov radiation in the visible region of the spectrum where it behaves like a dielectric. The CR dispersion relation in an isotropic medium such as silicon takes the form:

$$k_x^{cher} = \sqrt{\epsilon k_0^2 - (\omega/v_z)^2} \quad \text{and} \quad k_z = \frac{\omega}{v_z} \quad (S1)$$

where k_x^{cher} is the component of the CR wavevector ($k_{cherenkov}$) parallel to the sample interface and k_z is the component along the c-axis fixed by the electron velocity (v_z). CR radiates out in a cone with a Cherenkov cone angle (θ_c) between k_c and the axis of the electron trajectory (figure S2 (a)). Realizing $\tan(\theta_c) = k_x/k_z$, we define the cherenkov cone angle as:

$$\tan(\theta_c) = \sqrt{(v_z/c)^2 \epsilon - 1} \quad (S2)$$

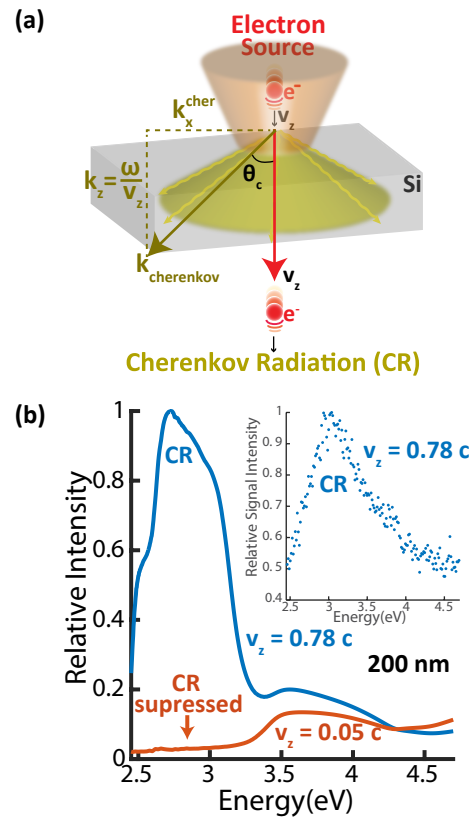


Fig. S2. Thin film Cherenkov radiation at large wavevectors (16-30 μ rad) in Si. (a) Schematic of CR excitation with wavevector $k_{cherenkov}$ (k_c) in silicon via an electron beam. θ_c is the Cherenkov cone angle (equation S2). (b) Theoretical energy loss function showing the relative electron loss intensity for a 200 nm silicon film integrated over the large scattering angle regime ($\theta = 16 - 30 \mu$ rad). The relative intensity above and below the Cherenkov velocity threshold is shown ($v_z = 0.78c$ (blue) and $v_z = 0.05c$ (red)) and CR is suppressed for the slow moving electron. Inset shows the corresponding integrated experimental measurement of CR via k -EELS for a 200 nm film at $v_z = 0.78c$.

For real values of θ_c , the electron velocity must be $v_z \geq c/\sqrt{\epsilon}$ which is defined as the CR velocity threshold. CR will only be

generated if the minimum electron velocity is the phase velocity in the medium.

The CR scattering probability in thin films decreases with decreasing thickness as it is captured by the volume energy loss function which is directly proportional to the sample thickness (d). This trend follows physical intuition as CR is a manifestation of the constructive interference of the fields in the bulk of the structure and thus suitably thick films are required to achieve coherent emission.

In figure 2 (b), (c), and (d) of the main manuscript, we note that the CR band is not as dispersive as the EUV surface plasmon but still clearly displays dispersive characteristics. This is evident from equation S1 and equation S2 where k_c and θ_c are highly dependent on v_z as well as the permittivity ϵ_{Si} (material response). Also, as is expected, the uncertainty in the band-structure measurement is seen to increase with increasing scattering angle and reduced sample thickness much like the plasmonic excitations (details in section 1B).

Figure S2 (b),(c) contrast the total energy loss function (both surface and volume contributions) integrated over large scattering angles ($16 - 30\mu\text{rad}$) above and below the CR velocity threshold for a 200 nm silicon film. We immediately note that strong peak which we classify as CR between 2.5-3.5 eV only exists when we are above the CR velocity threshold ($v_z \geq c/\sqrt{\epsilon}$). The peak between 3.5-4.2 eV is due to interband transitions in silicon [4] within this energy range and not a component of the CR excitation (as noted by the lack of suppression of the peak at slower velocities).

3. ANISOTROPIC CHERENKOV RADIATION DISPERSION IN UNIAXIAL MEDIA

A. Analytic Dispersion Relation

The anisotropic Cherenkov radiation dispersion in uniaxial media can be determined analytically from the uniaxial macroscopic electron energy loss function as defined in [5]. Specifically, anisotropic Cherenkov radiation is manifest in the volume loss contribution of the anisotropic energy loss function, which has the form: $ELF_{volume} \propto \frac{(1-\epsilon_x(v_z/c)^2)}{(\epsilon_x\phi_z^2)}d$ where v_z is the velocity of the source electron, d is the sample thickness, ϵ_x is the permittivity parallel to the interface and $\phi_z^2 = k_x^2 + (\epsilon_z/\epsilon_x)(\omega/v_z)^2 - \epsilon_z(\omega/c)^2$, where k_x is the wavevector parallel to the interface and ϵ_z is the permittivity perpendicular to the interface. We see that in the limit where $\phi_z = 0$, we get a resonantly large enhancement to our anisotropic energy loss function. This enhancement is a result of the anisotropic Cherenkov radiation in uniaxial media. We can determine the analytic uniaxial Cherenkov radiation dispersion by solving for the wavevector in the expression for ϕ_z^2 when $\phi_z = 0$:

$$k_x^c = \sqrt{\epsilon_z k_0^2 - \frac{\epsilon_z}{\epsilon_x} \left(\frac{\omega}{v_z}\right)^2} \quad \text{and} \quad k_z^c = \frac{\omega}{v_z} \quad (\text{S3})$$

where k_x^c is the component of the CR wavevector (k^c) parallel to the sample interface and k_z^c is the CR component along the c -axis fixed by the electron velocity (v_z). We define the anisotropic Cherenkov cone angle as seen in equation 1 and figure 4(a) of the main manuscript by realizing that $\tan(\theta_c) = k_x^c/k_z^c$.

B. Effective Medium Theory of a Uniaxial Structure Composed of an Si/SiO₂ Multilayer

In the main manuscript, alternating layers of crystalline silicon (c -Si) (permittivity shown in figure S1) and SiO₂ with permittivity

$\epsilon_{SiO_2} = 2.5$ are used to theoretically realize a uniaxial structure in the effective medium limit. Cherenkov radiation in such a structure would follow the dispersion relation defined in equation S3. We can define the effective permittivities for such a structure using the generalized Maxwell-Garnett approach for homogenization of a multilayer system (as seen in the appendix of [6]). The effective permittivities in the parallel (ϵ_x) and perpendicular (ϵ_z) directions are defined as:

$$\epsilon_x = \rho\epsilon_{Si} + (1 - \rho)\epsilon_{SiO_2} \quad (\text{S4})$$

$$\epsilon_z = \frac{\epsilon_{Si}\epsilon_{SiO_2}}{\rho\epsilon_{SiO_2} + (1 - \rho)\epsilon_{Si}} \quad (\text{S5})$$

where the fill fraction is defined as $\rho = d_{Si}/(d_{Si} + d_{SiO_2})$ and d_{Si} , d_{SiO_2} are the layer thicknesses of Si and SiO₂, respectively. For the simulations completed in the main manuscript, a fill fraction of $\rho = 0.35$ is used.

4. THRESHOLD REDUCTION OF CHERENKOV RADIATION IN HYPERBOLIC MEDIA AND TRADE-OFF WITH LOSS

The foundation of the thresholdless Cherenkov radiation (TCR) phenomena is due to the unique hyperbolic topology of the HMM isofrequency surface that can support infinitely large wavevectors in the ideal limit. We can map the different values of the CR wavevector (k_c) on the hyperbolic surfaces for different velocities of the electron source (note: $\tan(\theta_c) = k_x/k_z$). We see that in the limit that $v_z \rightarrow 0$ in equation 1 of the main manuscript, θ_c (and thus k^c) approaches the asymptotes of the hyperbola for both the type I and type II case (figure S3 (a)). In the ideal limit, infinitely large wavevectors can be supported at the asymptotes of the hyperbola and as such the phase velocity in the medium approaches 0 ($v_{phase} = \omega/k \rightarrow 0$). The minimum electron velocity where the CR condition is satisfied is at the point $v_z = v_{phase}$ and consequently the minimum CR velocity threshold is also $v_{th} \rightarrow 0$ in hyperbolic media.

One caveat to the unbounded velocity limit for CR in hyperbolic media is that we have an upper limit to the CR radiation condition in a type I HMM. This is due to the two sheeted nature of the type I hyperbola creating a bandgap in which photonic modes with wavevectors smaller than $k = k_0 * \sqrt{\epsilon_x}$ are not supported. As a result, any modes with $v_{phase} \geq c/\sqrt{\epsilon_x}$ cannot exist in type I HMMs leading to the upper CR cutoff in such structures. This upper TCR cutoff in type I HMMs ($v_z \leq c/\sqrt{\epsilon_x}$) is observed in figure 5 of the main manuscript where the TCR is suppressed at large v_z . Note that similar suppression does not occur in the type II region as it is truly thresholdless and no bandgap exists for the type II single-sheeted hyperboloidal isofrequency surface.

Figure S3 (b) shows the full field simulations of TCR in the type I and type II regimes of the Si/SiO₂ effective medium described in figure 4(a) of the main manuscript for electron velocities as low as $v_z = 0.001c$. In the ideal limit, the velocity has no lower limit, as indicated by figure S3 (a). However, two key factors limit the the threshold reduction of TCR in hyperbolic media: (1) the material loss and (2) the size of the unit cell of the multilayer structure.

The material loss and nonlocal effects greatly damp the high- k modes of hyperbolic media at large k and thus the phase velocity in the medium can never truly reach 0. As a result, we know that the threshold reduction is fundamentally limited by the

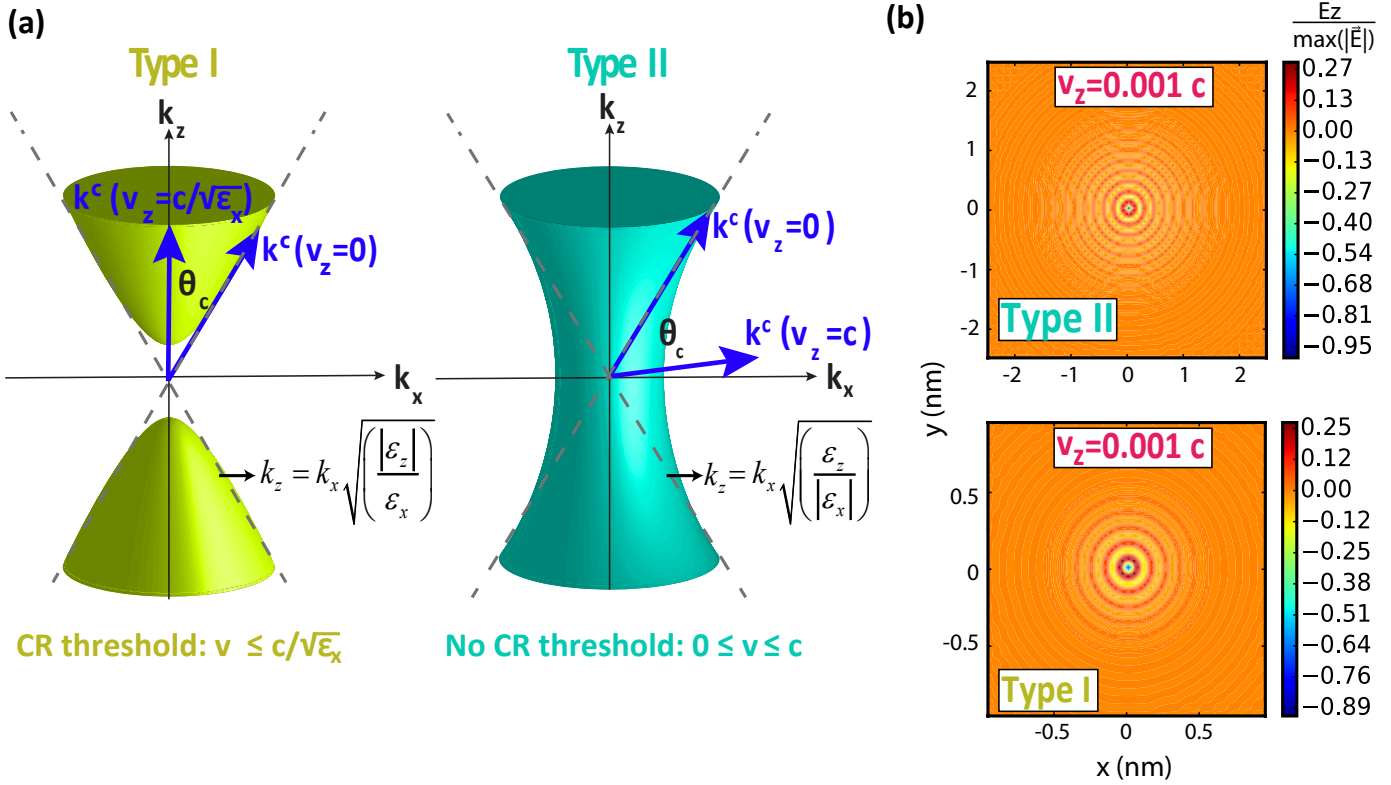


Fig. S3. (a) The type I ($\epsilon_x > 0, \epsilon_z < 0$) and type II ($\epsilon_x < 0, \epsilon_z > 0$) isofrequency surfaces for HMMs that can support thresholdless cherenkov radiation (TCR) with a wavevector k_c . The dashed lines show the asymptotes of the hyperbola and correspond to the k_c for which the Cherenkov velocity threshold is $v_z = 0$. This is where infinitely large wavevectors are supported in a hyperbolic medium and thus $v_{phase} = \omega/k \rightarrow 0$ and the Cherenkov velocity threshold is eliminated. (b) Full field simulations of the type I and type II thresholdless Cherenkov radiation of the Si/SiO₂ effective medium described in figure 4(a) of the main manuscript at velocities as low as $v_z = 0.001c$. In the ideal limit the TCR has no lower velocity threshold as seen in (a). However, material loss in the structure as well as the finite size of the unit cell of a real multilayer structure fundamentally limit the reduction of the phase velocity in the medium and thus limit the Cherenkov velocity threshold reduction.

ability to reduce the phase velocity, and the minimum threshold velocity is $v_{th} = v_{phase}$.

Additionally, the fundamental lower velocity limit will be governed by the wavelength limit at which the medium ceases to act as an effective medium. Figure S3 (b) display the electric fields for a true effective medium and not a realistic multilayer structure which would have a finite unit cell size. The finite unit cell size limits the extent of the high- k modes supported by the structure to the edges of the brillioun zone and as a result, limits the reduction of the phase velocity in the medium.

REFERENCES

1. M. Bergen, M. Malac, R. McLeod, D. Hoyle, Y. Taniguchi, T. Yaguchi, J. Chen, and T. Yotsuji, "Centralized Instrument Control for a TEM Laboratory," *Microsc. Microanal.* **19**, 1394–1395 (2013).
2. G. Kresse and J. Furthmüller, "Efficient iterative schemes for ab initio total-energy calculations using a plane-wave basis set," *Phys. Rev. B* **54**, 11169–11186 (1996).
3. E. D. Palik, *Handbook of Optical Constants of Solids* (Academic Press, 1998).
4. H. R. Philipp and H. Ehrenreich, "Optical Properties of Semiconductors," *Phys. Rev.* **129**, 1550–1560 (1963).
5. C. H. Chen and J. Silcox, "Calculations of the electron-energy-loss probability in thin uniaxial crystals at oblique incidence," *Phys. Rev. B* **20**, 3605–3614 (1979).
6. P. Shekhar, J. Atkinson, and Z. Jacob, "Hyperbolic metamaterials: fundamentals and applications," *Nano Convergence* **1**, 1–17 (2014).